Optics Letters

Laser-diode pumped self-mode-locked praseodymium visible lasers with multi-gigahertz repetition rate

Yuxia Zhang,[1] Haohai Yu,[1,*] Huaijin Zhang,[1,3] Alberto Di Lieto,[2] Mauro Tonelli,[2] and Jiyang Wang[1]

[1]State Key Laboratory of Crystal Materials and Institute of Crystal Materials, Shandong University, Jinan 250100, China
[2]NEST Istituto Nanoscienze-CNR and Dipartimento di Fisica dell'Università di Pisa, Largo B. Pontecorvo 3, 56127 Pisa, Italy
[3]e-mail: huaijinzhang@sdu.edu.cn
*Corresponding author: haohaiyu@sdu.edu.cn

Received 19 April 2016; revised 14 May 2016; accepted 17 May 2016; posted 17 May 2016 (Doc. ID 263516); published 2 June 2016

We demonstrate efficient laser-diode pumped multi-gigahertz (GHz) self-mode-locked praseodymium (Pr^{3+}) visible lasers with broadband spectra from green to deep red for the first time to our knowledge. With a Pr^{3+}-doped $GdLiF_4$ crystal, stable self-mode-locked visible pulsed lasers at the wavelengths of 522 nm, 607 nm, 639 nm, and 720 nm have been obtained with the repetition rates of 2.8 GHz, 3.1 GHz, 3.1 GHz, and 3.0 GHz, respectively. The maximum output power was 612 mW with the slope efficiency of 46.9% at 639 nm. The mode-locking mechanism was theoretically analyzed. The stable second-harmonic mode-locking with doubled repetition frequency was also realized based on the Fabry–Perot effect formed in the laser cavity. In addition, we find that the polarization directions were turned with lasing wavelengths. This work may provide a new way for generating efficient ultrafast pulses with high- and changeable-repetition rates in the visible range.

OCIS codes: (140.3480) Lasers, diode-pumped; (140.3580) Lasers, solid-state; (140.4050) Mode-locked lasers; (140.7300) Visible lasers.

http://dx.doi.org/10.1364/OL.41.002692

Trivalent praseodymium (Pr^{3+}) ions have rich energy level distributions and can emit broadband visible spectra from green to deep red by the electron transition between different energy levels [1,2]. With the development of blue laser diodes (LDs), Pr^{3+}-doped crystals have gradually attracted more and more attention, since they have been identified as one of the most potential gain materials of diode-pumped all-solid-state visible lasers [3,4]. In recent years, blue LD-pumped Pr^{3+}-doped crystal visible lasers have achieved tremendous progress in continuous-wave (cw) operations, and high efficiency cw Pr^{3+} ion visible lasers have been widely studied with the slope efficiencies close to the theoretical maximum at the wavelengths of 522 and 639 nm [5]. In pulse laser experiments, LD-pumped Q-switched Pr^{3+} ion visible lasers with kilohertz repetition rates and nanosecond pulse widths have been reported [6,7]. With argon-ion lasers as the pump sources, the first Kerr-lens mode-locked Pr^{3+}:$YLiF_4$ visible lasers were realized with the Kerr-lens effect and initiated by saturable absorbers in 1994 [8]. The first self-staring Kerr-lens mode-locked Pr^{3+}:$YLiF_4$ laser was reported in 1996, which was also pumped by an argon-ion laser [9]. In 2014, with a intracavity frequency-doubled optically pumped InGaAs semiconductor disk laser (2ω-OPSL) as the pump source, the self-starting stable cw mode-locked Pr^{3+} ion visible laser at the wavelength of 639 nm was first reported with a SESAM as the saturable absorber [10]. Therefore, up to now, there are no reports on the generation of mode-locked Pr^{3+} ion visible lasers with a blue LD as the pump source to the best of our knowledge. In recent years, the self-mode-locking of Nd^{3+}- and Yb^{3+}-doped crystal lasers with GHz repetition rates and picosecond/femtosecond pulse widths has been widely reported based on simple two-mirror cavities [11–13] and was proposed to have promising applications, which is the motivation for investigating the self-mode-locking of Pr^{3+}-doped visible lasers.

In this Letter, with a blue LD as the pump source, all-solid-state self-mode-locked multi-GHz visible lasers are demonstrated with Pr^{3+}-doped $GdLiF_4$ (Pr:GLF) crystal at wavelengths from 522 to 720 nm based on a short laser cavity. The pulse widths were about dozens of picoseconds corresponding to repetition rates of 3 GHz. Besides, the second-harmonic mode-locking was generated with a repetition rate about 5.6 GHz, which was dependent on the external F–P cavity formed by the end face of the crystal and cavity mirror [14]. We also propose that these multi-GHz visible lasers may have some special applications in some emerging fields, including the superconducting single-photon detector [15], electro-optic sampling [16], high-speed soliton communication and thin-film metrology by picosecond ultrasonics [17], generation of ultraviolet, even deep ultraviolet, high-repetition-rate ultrafast lasers by direct frequency doubling [18], etc.

For the Pr^{3+}-doped crystal, the emission spectrum covers wavelengths ranging from green to deep red, corresponding to different electron transitions between different energy levels. The polarized emission cross sections of the Pr:GLF crystal are

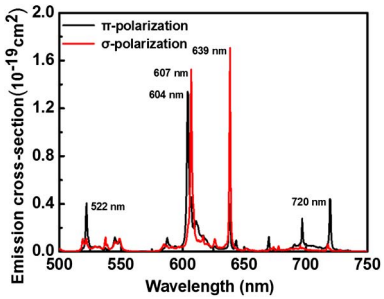

Fig. 1. Polarized emission spectra of Pr:GLF crystal.

shown in Fig. 1. In this figure, the emission spectra are anisotropic and the strongest emission peaks are located at 522 nm, 604/607 nm, 639 nm, and 720 nm. Compared with the different polarized spectra, it can be observed that π polarization emission cross sections are larger than those of σ polarization at the wavelengths of 522 nm and 720 nm. However, this situation changes at the wavelengths of 604/607 nm and 639 nm. It should also be noted that the wavelength of π polarization is 604 nm and that of σ polarization is 607 nm from $^3P_0$ to $^3H_6$ [3]. The results indicate that for the efficient generation of Pr:GLF crystal lasers, the polarization should be different and the optimized π polarization is the wavelengths of 522 nm and 720 nm, and the optimized σ polarization is the wavelengths of 607 nm and 639 nm.

A simple two-mirror cavity was used in multi-GHz self-mode-locked experiments. The experimental schematic is shown in Fig. 2. The laser cavity was a compact plano-concave cavity without any additional components. A 445 nm blue LD with a maximum output power of 1.86 W was employed as the pump source. The gain medium was a 1.01 at. % Pr:GLF crystal cut along its a direction with dimensions of $2.7 \times 3.2 \times 6.9$ mm^3 ($a \times c \times a$). Both of the end surfaces were polished and antireflection coated at the wavelength of 445 nm and wavelengths range from 500 nm to 720 nm. In order to remove the generated heat, the Pr:GLF crystal was wrapped by an indium foil and mounted in a water-cooled copper block. The water temperature was maintained at 7°C. The blue pump light was focused into the gain crystal by a focal lens with a focal length of 25 mm. M1 was a plane mirror with antireflection coating at 445 nm and highly reflective coating at the wavelengths range from 500 to 750 nm. In order to generate lasers at the different wavelengths, various output couplers M2 were chosen and all mirrors were concave mirrors with radii of curvature of 50 mm. By changing the output coupler M2, green, orange, red, and deep red lasers were obtained at the

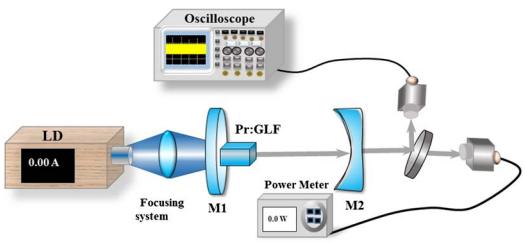

Fig. 2. Experimental configuration of a diode-pumped self-mode-locked Pr:GLF visible laser.

wavelengths of 522 nm, 607 nm, 639 nm, and 720 nm, respectively. The mode-locked pulse trains were detected by an InGaAs photodetector (New focus, 1414 model) with a rise time of 14 ps and recorded by a digital oscilloscope (Tektronix, MSO 72504DX) with an electrical bandwidth of 25 GHz and a rise time of 16 ps. The laser spectra were monitored by a spectrometer (YOKOGAWA, AQ6315) with a resolution of 0.05 nm.

In order to ensure the high circulating intracavity power, the transmission of output couplers should be low under the high-conversion-efficiency condition. In the experiments, all the transmission of output couplers was optimized to be less than 2% at the oscillating wavelength. Based on the emission spectra shown in Fig. 1, the emission cross-sections are different at different wavelengths. Therefore, in order to generate lasers with small emission cross sections, some strong emission should be suppressed. For the green laser, M2 was chosen to be partially reflection coated with a transmissivity of 2% at 522 nm and high transmission (HT) coating at 600–750 nm for suppressing the emission under this wavelength band. For the orange laser, the transmissivity of the output coupler was 1% at the wavelength of 607 nm and HT coating at 630–750 nm. For the red laser, the transmissivity of M2 was designed to be 1.8% at 639 nm and HT coating at 650–750 nm, and for the deep red laser at the wavelength of 720 nm, the transmissivity M2 was chosen to be 1.4% at 720 nm and HT coating at wavelengths under 700 nm.

Based on the theoretical model of thermal-Kerr self-mode locking developed by Xie *et al.* [19], the modulation by the thermal induced diffraction loss and saturable gain are mode-size dependent and should be responsible for the self-mode-locking process. At the self-mode-locking process, the thermal lens would generate the phase distortion and loss, which can be modulated by the Kerr lens, and the saturable gain is associated with the soft gain aperture effect [19–22]. With the Kerr self-focusing theory [21] and ABCD matrix formulation, the mode size change of our experiment was calculated to be about 0.1 μm at the pump power of 1 W, which leads to a round-trip diffraction loss modulation of 2×10^{-3}. Meanwhile, the saturation intensity of our laser experiment is about 160 kW/cm^2 and the average laser intensity in this crystal is calculated to be about 670 kW/cm^2. Thus, with the 0.1 μm mode size change, the gain modulation is 5×10^{-4}. Besides, the self-starting condition can be given by [23]

$$L_{nl} > \pi T_R \Delta\nu / \ln(m), \tag{1}$$

where L_{nl} is the nonlinear loss modulation, T_R is the round-trip time, $\Delta\nu$ is 3 dB width of the first beat note of the axial modes, and m is the number of modes initially oscillating. For our experiment, $\Delta\nu$ is measured to be 12 kHz and the round-trip time is about 26 ns. Assuming $\ln(m) = 3$, the nonlinear loss modulation would be calculated as $L_{nl} > 3 \times 10^{-6}$. Based on the calculation above, the total modulation caused by the round-trip diffraction loss and average gain are about 2 orders of magnitude larger than the threshold value L_{nl}, which means that the present configuration can generate self-starting mode-locking.

During the experimental process, by rotating Pr:GLF crystal about 5° from the normal direction of the cavity, the F–P cavity formed by the surface of the crystal and the mirrors were suppressed and the self-mode-locking with the repetition rate

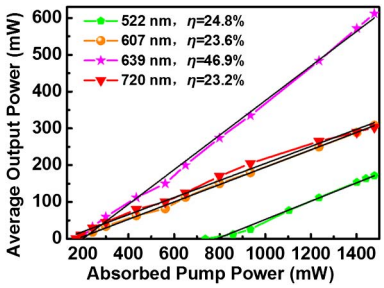

Fig. 3. Average output power versus absorbed pump power in self-mode-locked operation at 522 nm, 607 nm, 639 nm, and 720 nm.

about 3 GHz appeared when the pump power exceeded the lasing threshold by appropriately adjusting the laser cavity. The Q-switched mode-locking was not observed in the experiment and this phenomenon also appeared in the near-infrared GHz self-mode-locking with a two-mirror short cavity [11,12]. The average output power at these four wavelengths are shown in Fig. 3. The absorbed pump power thresholds were measured to be 737 mW at the wavelength of 522 nm, 191 mW at the wavelength of 607 nm, 172 mW at the wavelength of 639 nm, and 165 mW at the wavelength of 720 nm. The average output power was observed to be linearly increased with the increase of the absorbed pump power. The slope efficiency was 24.8%, 23.6%, 46.9%, and 23.2% at the wavelength of 522 nm, 607 nm, 639 nm, and 720 nm, respectively, which was comparable with the previously reported continuous-wave visible lasers [3]. The maximum output power was 172 mW at 522 nm, 308 mW at 607 nm, 612 mW at 639 nm, and 303 mW at 720 nm under the absorbed pump power of 1.48 W. It should be noted that measured with a polarizer, the different wavelengths corresponded to different polarizations: π polarization at the wavelengths of 522 nm and 720 nm, and σ polarization at the wavelengths of 607 nm and 639 nm, which agreed well with that measured in the spectra shown in Fig. 1.

The representatives of self-mode-locked pulse trains at different wavelengths in the time span of 4 ns were shown in Figs. 4(a)–4(d), respectively. From these figures, it could be found that the repetition rates were 2.8 GHz, 3.1 GHz, 3.1 GHz, and 3.03 GHz at the wavelengths of 522 nm, 607 nm, 639 nm, and 720 nm, respectively. The little difference in the repetition rates should be generated by slightly tuning for the stable mode-locking. It can also be found that the mode-locked pulse trains were fully modulated without cw background. The pulse widths were 72 ps, 69 ps, 53 ps, and 74 ps at the wavelength of 522 nm, 607 nm, 639 nm, and 720 nm, respectively. The pulse width at the wavelength of 639 nm (53 ps) was also confirmed by a homemade autocorrelator with a β-BBO nonlinear crystal, and the result is similar with the pulse width achieved with the oscilloscope (16 ps rise time) and the high speed detector (14 ps rise time). The radio frequency (RF) spectra were measured and the typical result at the wavelength of 720 nm was shown in Fig. 4(f) with a 100 kHz resolution bandwidth. As can be seen in Fig. 4(f), the signal-to-noise was about 62 dB above the background level and the corresponding center repetition frequency was 3.03 GHz. The typical self-mode-locked pulse trains at the wavelength of 607 nm in the time span of 40 μs was shown

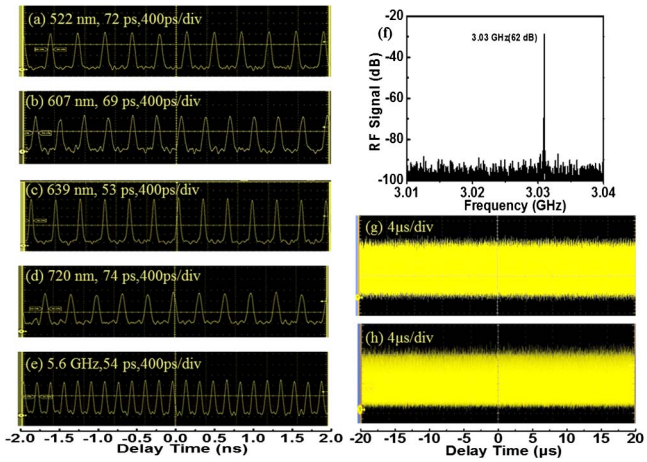

Fig. 4. Experimental self-mode-locked pulse trains observed in different time scopes and different wavelengths: (a)–(d) pulse trains observed in the time scope of 4 ns at the wavelength of 522 nm, 607 nm, 639 nm, and 720 nm, respectively; (e) pulse train with the repetition rate of 5.6 GHz corresponding to a pulsed width of 54 ps; (f) typical RF spectrum with a frequency of 3.03 GHz measured at the wavelength of 720 nm; (g) and (h) the pulse trains observed in the time scope of 40 μs with the repetition rate of 2.8 GHz and 5.6 GHz, respectively.

in Fig. 4(g). Observed under long time spans, we found that the amplitude of self-mode-locked pulse trains exhibited smooth, which indicated that the relaxation oscillations were well suppressed and the mode-locking was stable without the effect of mode beating. In order to get high-order harmonic mode-locking, the laser crystal was rotated to be parallel to the normal direction of the cavity. Under this condition, the F–P cavity can be formed by the surface of the crystal and the cavity mirrors and can cut the round-trip time [20]. By calculation, we got that the ratio between the optical length of the crystal and the length from the end face of the crystal to the output coupler was 0.5 at 522 nm, which means that the second harmonic mode-locking can be achieved with the repetition rate of 5.6 GHz in agreement with the previous results reported in the Nd^{3+}-doped crystal and glass lasers [14,24]. The pulse trains in the time span of 4 ns and 40 μs with a repetition rate of 5.6 GHz and a pulse width of 54 ps were shown in Figs. 4(e) and 4(h), respectively, with almost unchanged output power.

Measured with a spectrometer, the mode-locked spectra were shown in Fig. 5, with the center wavelength of 522.56 nm, 607.59 nm, 639.15 nm, and 720.46 nm, and the corresponding full width at half maximum (FWHM) were 0.11 nm, 0.17 nm, 0.19 nm, and 0.19 nm, respectively. The relatively high time-bandwidth production should be related to the relatively low resolution (0.05 nm) of the used spectrometer. The characterization about the self-mode-locking was shown in Table 1 to be clear.

In conclusion, based on the spectral analysis and the physics of self-mode-locking, we have experimentally realized the efficient LD pumped self-mode-locked visible lasers at a wavelength range from 522 nm to 720 nm. The wavelengths covered from the green to deep red spectra, which should have some promising applications based on the visibility, high efficiency, ultrahigh repetition rate, and ultrashort pulse width.

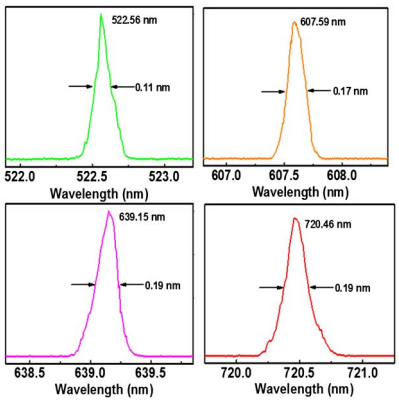

Fig. 5. Measured spectra of the self-mode-locked visible laser at the central wavelengths of 522.56 nm, 607.59 nm, 639.15 nm, and 720.58 nm.

Table 1. Measured Data at Four Different Wavelengths

Wavelength (nm)	522.56	607.59	639.15	720.46
Polarization	π	σ	σ	π
Transmissivity (%)	2	1	1.8	1.4
Slope efficiency (%)	24.8	23.6	46.9	23.2
Output power (mW)	172	308	612	303
Pulse width (ps)	72	69	53	74
Repetition rate (GHz)	2.8	3.1	3.1	3.0
FWHM (nm)	0.11	0.17	0.19	0.19

With Pr:GLF crystal as the gain material, the self-mode-locked pulse visible lasers with the repetition rate of 3 GHz and the pulse width of tens of picoseconds were generated in a simple cavity without any additional modulator except for the gain medium inside the laser cavity. The maximum efficiency was 46.9% and the maximum output power was 612 mW at the wavelength of 639 nm. In addition, by employing an F–P cavity formed by the refection of surfaces, the second-harmonic mode-locking was also achieved with the doubled repetition rate. All self-mode-locked lasers were linearly polarized, but with different polarization. In addition, by considering the fluorescence peaks of the Pr:GLF crystal with a width of about 1 nm, we propose that the LD pumped mode-locked visible lasers with widths of 100 fs should be possible by suitable dispersion compensation [25], which should have more promising applications in some fields similar to discovering the nature of plasmonics, such as damping of acoustic vibrations [26,27].

Funding. National Natural Science Foundation of China (NSFC) (51422205, 51372139, 51272131); The Natural Science Foundation for Distinguished Young Scholars of Shandong Province (JQ201415); Taishan Scholar Foundation of Shandong Province, China.

REFERENCES

1. L. Esterowitz, F. Bartoli, R. Allen, D. Wortman, C. Morrison, and R. Leavitt, Phys. Rev. B **19**, 6442 (1979).
2. T. Sandrock, T. Danger, E. Heumann, G. Huber, and B. Chai, Appl. Phys. B **58**, 149 (1994).
3. F. Cornacchia, A. Di Lieto, M. Tonelli, A. Richter, E. Heumann, and G. Huber, Opt. Express **16**, 15932 (2008).
4. F. Cornacchia, A. Richter, E. Heumann, G. Huber, D. Parisi, and M. Tonelli, Opt. Express **15**, 992 (2007).
5. T. Gün, P. Metz, and G. Huber, Opt. Lett. **36**, 1002 (2011).
6. J. Kojou, R. Abe, R. Kariyama, H. Tanaka, A. Sakurai, Y. Watanabe, and F. Kannari, Appl. Opt. **53**, 2030 (2014).
7. R. Abe, J. Kojou, K. Masuda, and F. Kannari, Appl. Phys. Express **6**, 032703 (2013).
8. S. Ruan, J. Sutherland, P. French, J. Taylor, and B. Chai, Electron. Lett. **30**, 1601 (1994).
9. Y. Tong, J. Sutherland, P. French, J. Taylor, A. Shestakov, and B. Chai, Opt. Lett. **21**, 644 (1996).
10. M. Gaponenko, P. W. Metz, A. Härkönen, A. Heuer, T. Leinonen, M. Guina, T. Südmeyer, G. Huber, and C. Kränkel, Opt. Lett. **39**, 6939 (2014).
11. H. Liang, Y. Huang, W. Huang, K. Su, and Y. Chen, Opt. Lett. **35**, 4 (2010).
12. Y. Huang, Y. Tzeng, C. Tang, Y. Huang, and Y. Chen, Opt. Express **20**, 18230 (2012).
13. W. Zhuang, M. Chang, H. Liang, and Y. Chen, Opt. Lett. **38**, 2596 (2013).
14. Y. Chen, M. Chang, W. Zhuang, K. Su, K. Huang, and H. Liang, Laser Photon. Rev. **9**, 91 (2015).
15. G. Goltsman, O. Minaeva, A. Korneev, M. Tarkhov, I. Rubtsova, A. Divochiy, I. Milostnaya, G. Chulkova, N. Kaurova, B. Voronov, D. Pan, J. Kitaygorsky, A. Cross, A. Pearlman, I. Komissarov, W. Slysz, M. Wegrzecki, P. Grabiec, and R. Sobolewski, IEEE Trans. Appl. Supercond. **17**, 246 (2007).
16. K. Weingarten, M. Rodwel, and D. Bloom, IEEE J. Quantum Electron. **24**, 198 (1988).
17. M. Fermann, A. Galvanauskas, and G. Sucha, *Ultrafast Lasers: Technology and Applications* (CRC Press, 2002).
18. J. Kleinbauer, R. Knappe, and R. Wallenstein, Appl. Phys. B **80**, 315 (2005).
19. G. Xie, D. Tang, L. Zhao, L. Qian, and K. Ueda, Opt. Lett. **32**, 2741 (2007).
20. K. Liu, C. Flood, D. Walker, and H. Driel, Opt. Lett. **17**, 1361 (1992).
21. M. Piché, Opt. Commun. **86**, 156 (1991).
22. S. Tidwell, J. Seamans, M. Bowers, and A. Cousins, IEEE J. Quantum Electron. **28**, 997 (1992).
23. G. Cerullo, S. Desilvestri, and V. Magni, Opt. Lett. **19**, 1040 (1994).
24. G. Xie, L. Qian, H. Zhu, and H. Yang, J. Korean Phys. Soc. **49**, 1438 (2006).
25. J. Sutherland, P. French, J. Taylor, and B. Chai, Opt. Lett. **21**, 797 (1996).
26. T. Kelf, Y. Tanaka, O. Matsuda, E. Larsson, D. Sutherland, and O. Wright, Nano Lett. **11**, 3893 (2011).
27. M. Pelton, J. E. Sader, J. Burgin, M. Liu, P. Guyot-Sionnest, and D. Gosztola, Nat. Nanotechnol. **4**, 492 (2009).